Analyst

RSC Publishing

PAPER

View Article Online
View Journal | View Issue

Cite this: *Analyst*, 2013, **138**, 6323

A novel aptamer-based competition strategy for ultrasensitive electrochemical detection of leukemia cells†

Kui Zhang,‡[ab] Tingting Tan,‡[ab] Jia-Ju Fu,[b] Tingting Zheng[b] and Jun-Jie Zhu*[b]

Received 30th June 2013
Accepted 3rd August 2013

DOI: 10.1039/c3an01255g

www.rsc.org/analyst

A robust, nanobiotechnology-based electrochemical cytosensing platform for the detection of acute leukemia cells was developed with high sensitivity, selectivity, acceptable rapidity and excellent extensibility. It utilized the competitive binding of cell-specific aptamers to acute leukemia cells and subsequent voltammetric quantification of the metal signature. Greatly enhanced sensitivity was achieved with dual signal amplification by using Fe_3O_4 magnetic nanoparticles (MNPs) as carriers to load a large amount of gold nanoparticles (AuNPs) and AuNP-catalyzed silver deposition. The proposed competitive cytosensor showed high sensitivity with a detection limit down to 10 cells. This simple and low-cost electrochemical cytosensing approach offers great promise to extend its application to early detection of human leukemia and possibly to other cancer cells.

Introduction

Acute leukemia is the most common pediatric malignancy and remains the leading cause of disease-related mortality in children and adolescents.[1] Acute leukemia has a rapid clinical course and progresses over several weeks to months, ultimately culminating in bone marrow failure.[2] Therefore, the early and accurate diagnosis is critical for improving patient survival rate. The identification and quantification of leukemia cells, which is directly related to diagnosis, have become a foundation of therapy and a means of evaluating the therapeutic effect.

To date, some methods for the detection of leukemia cells have been reported, such as flow cytometry,[3] immunohistochemistry,[4] polymerase chain reaction,[5] microarray,[6] and cell enrichment.[7] However, these methods may be relatively costly, time-consuming, labor-intensive, or require sophisticated instrumentation, which results in many leukemias being diagnosed at an advanced stage or even after metastasis throughout the body. Consequently, it is still a major challenge to develop innovative and appropriate detection approaches to overcome the limitations associated with the conventional methods mentioned above. The electrochemical sensing technique, with its intrinsic advantages of high sensitivity, simple operability, rapid response, and low cost, has attracted increasing attention.[8,9] The competition assay has the potential to identify ligands with high affinity for the target, reduce the problem of false-positive results, and enhance the detection selectivity.[10–13] It could also be introduced into the construction and optimization of the sensing method. For instance, Lang *et al.*[14] designed a cytometry-based competition assay to determine peptide affinity for HLA class II molecules and discriminate strong, moderate and poor HLA-DP binders. Wang *et al.*[15] developed a three-layer, competition-based, giant magnetoresistive assay to detect urinary endoglin with high specificity, and distinguish between different grades of prostate cancer. Incorporation of the competition assay into electrochemical sensing could provide a new method for detection of leukemia cells, which are generally present at extremely low concentrations and might otherwise go unnoticed, with better selectivity and higher sensitivity.

Target molecular recognition plays a vital role in the development of the competition assay. Owing to the high affinity and specificity towards a variety of target molecules, including metal ions, proteins and whole cells,[16–18] aptamers are promising molecular recognition elements. Aptamers are short single-stranded oligonucleotides and selected from nucleic acid libraries *via* an *in vitro* evolution process called SELEX (systematic evolution of ligands by exponential enrichment).[19,20] When a target molecule is introduced, the aptamer undergoes structure switching to bind the target, generating a detectable response signal and offering a good starting point for the development of the sensing method.[8,21,22] In addition to their desirable binding capability, aptamers are useful molecular tools with many other significant advantages over traditional antibodies, such as ease of synthesis, tailored binding affinity,

[a]*The Affiliated Drum Tower Hospital of Nanjing University Medical School, Nanjing University, Nanjing, 210008, P. R. China*

[b]*State Key Laboratory of Analytical Chemistry for Life Science, School of Chemistry and Chemical Engineering, Nanjing University, Nanjing, 210093, P. R. China. E-mail: jjzhu@nju.edu.cn*

† Electronic supplementary information (ESI) available: Fig. S1A–C. See DOI: 10.1039/c3an01255g

‡ These authors contributed equally to this work.

and lower vulnerability to denaturation.[23,24] Hence, they are endowed with great potential for selective recognition and detection of target leukemia cells.

Considering the low concentration of leukemia cells at early stages of the disease, there is an obvious need to develop a signal amplification route, so as to enhance the detection sensitivity. Fe_3O_4 MNPs, with a high surface-to-volume ratio, easily modified surface, and good biocompatibility, are well suited to serve as nanocarriers for loading nanomaterials and biomolecules.[25] Besides, for the superparamagnetic property, using an external magnetic field to extract directly the Fe_3O_4 MNPs from complex samples, without pre-enrichment or purification, could simplify the assay and reduce the background interference. Given the attractive characteristics of high sensitivity, low cost, and no need for sophisticated apparatus,[26] AuNP-catalyzed silver deposition enhancement, which is competitive with other signal amplification routes, such as phosphatase- and redox cycling-based signal amplification[27] and multilabeled QD-based signal amplification,[28] has been widely used in histochemical microscopy for sensitivity improvement.[29] It can also be developed in connection with the measurement of the deposited silver by electrochemical stripping.[30] As noted above, we developed a dual signal amplification strategy that integrated the signal amplification using Fe_3O_4 MNPs as strong nanocarriers to load a large amount of AuNPs, and further amplification by AuNP-catalyzed silver deposition. The sensitivity of the target molecular detection can be dramatically enhanced for a low detection limit.

Here, we took advantage of the target-binding-induced, structure-switching aptamer that can preferentially form an aptamer–target complex after competitive binding, and magnetic enrichment and separation technology, to form an innovative, competitive, hybridization-based electrochemical sensing platform for ultrasensitive detection of low-abundance leukemia cells. This strategy facilitated the integration of different functional elements into a synergetic detection method to achieve efficient analysis of target analytes: the inherent high sensitivity of the electrochemical technique; high selectivity of the competition assay; unique structure-switching ability and specific target-recognition capability of aptamers; convenient operation by magnetic separation; and dual signal amplification based on Fe_3O_4 MNPs carrying AuNPs and AuNP-catalyzed silver deposition. To demonstrate the new method, CCRF-CEM acute leukemia cells were chosen as model cells.

Experimental

Materials and reagents

1-Ethyl-3-(3-dimethylaminopropyl)carbodiimide hydrochloride (EDC), *N*-hydroxysuccinimide (NHS), tris-(2-carboxyethyl)phosphine hydrochloride (TCEP), silver enhancer solution A and B (SE-100), sodium thiosulfate pentahydrate ($Na_2S_2O_3 \cdot 5H_2O$), and calcein acetoxymethyl ester (calcein-AM) were obtained from Sigma-Aldrich (St. Louis, MO, USA). Chloroauric acid ($HAuCl_4 \cdot 4H_2O$) and trisodium citrate were obtained from Shanghai Chemical Reagent Co. Ltd. (Shanghai, China). Iron trichloride hexahydrate ($FeCl_3 \cdot 6H_2O$), ethylene glycol (EG), anhydrous NaAc, polyacrylic acid (PAA), tris-(hydroxymethyl)-aminomethane (Tris), and NaCl were purchased from Nanjing Chemical Reagent Co. Ltd. (Nanjing, China). All other chemical reagents were of analytical grade and used without further purification. Dulbecco's Phosphate-Buffered Saline (D-PBS, pH 7.4) comprised 0.90 mM $CaCl_2$, 0.49 mM $MgCl_2$, 137.93 mM NaCl, 2.67 mM KCl, 8.06 mM Na_2HPO_4, and 1.47 mM KH_2PO_4. All aqueous solutions were prepared with ultrapure water ($\geq$18 MΩ, Milli-Q, Millipore Simplicity, USA).

All the oligonucleotides were synthesized by Shanghai Sangon Biotechnology Co. Ltd. (Shanghai, China). The sequence of 5′-NH_2-modified aptamer for CCRF-CEM cells was 5′-NH_2-ATC TAA CTG CTG CGC CGC CGG GAA AAT ACT GTA CGG TTA GA-3′.[31] The sequence of 5′-SH-modified partial complementary DNA (cDNA) was 5′-SH-TTT TTT-TAA CCG TAC AGT-3′.

Apparatus

All electrochemical experiments were performed on a CHI832B electrochemical analyzer (Shanghai Chenhua, Shanghai, China). All square wave stripping voltammetric measurements were carried out using a conventional three-electrode system with a glassy carbon electrode (GCE) as the working electrode, a saturated calomel electrode (SCE) as the reference, and a platinum wire as the auxiliary. Fluorescence microscopy was performed using a Nikon TE2000-U inverted optical microscope (Tokyo, Japan). Scanning electron microscopy (SEM) images were obtained using a field-emission scanning electron microscope (Hitachi S4800, Japan). The morphology of the cDNA–AuNP nanoconjugates was characterized by transmission electron microscopy (TEM; JEM-1011, Jeol, Tokyo, Japan). Fourier transform infrared (FT-IR) spectra were recorded on a Nicolet 6700 FT-IR spectrometer (Thermo Fisher Scientific, USA) using the KBr method. Ultraviolet-visible (UV-vis) absorption spectra were recorded on a Shimadzu UV-3600 spectrophotometer (Kyoto, Japan).

Preparation of carboxyl-functionalized Fe_3O_4 MNPs

The carboxyl-functionalized Fe_3O_4 MNPs were prepared by hydrothermal treatment as previously described.[32] $FeCl_3 \cdot 6H_2O$ (1.35 g) was dissolved in EG (38 mL) to form a transparent solution, followed by the addition of anhydrous NaAc (3.2 g) and PAA (0.5 mL). The mixture was stirred vigorously and ultrasonicated at room temperature for 30 min to obtain a homogeneous solution. This solution was then transferred into a Teflon-lined stainless steel autoclave and reacted at 200 °C for 6 h. After the autoclave was cooled to room temperature, the products were separated from the supernatant using magnetic force, rinsed alternately three times with deionized water and ethanol, and then dried at 50 °C for 6 h in a vacuum drying oven before application.

Synthesis of aptamer–Fe_3O_4 MNP nanoconjugates

Briefly, 0.2 mg of the as-prepared carboxyl-functionalized Fe_3O_4 MNPs were resuspended in 1 mL D-PBS (pH 7.4) buffer, and ultrasonicated for 10 min. Then, 2 mg EDC and 2 mg NHS dissolved in 1 mL D-PBS buffer were mixed with the Fe_3O_4 MNP

suspension with stirring at room temperature for 1 h to activate the terminal carboxyl group on the surface of Fe_3O_4 MNPs. In order to dissociate any pre-existing higher-order structures, prior to use, aptamers should be thermally treated at 95 °C for 3 min, followed by cooling for 10 min. A total of 5 μL (20 μM) amino-modified aptamer was added to the mixture and stirred at 37 °C for 2 h to immobilize the aptamers on the Fe_3O_4 MNP surface, followed by a blocking step with 1 M ethanolamine for 1 h to minimize nonspecific interference. After magnetic separation with an external magnet, the resulting aptamer–Fe_3O_4 MNP nanoconjugates were washed three times with D-PBS buffer to remove the free amino-modified aptamers, dispersed in 100 μL D-PBS buffer and stored at 4 °C.

Preparation of AuNPs and cDNA–AuNP nanoconjugates

The synthesis of AuNPs was adapted from a previously described method.[33,34] All the glassware and magnetic stir bar should be soaked in *aqua regia* (HCl–HNO_3 3 : 1) for at least 1 h, rinsed with copious amount of ultrapure water, and oven-dried prior to use (safety note: the *aqua regia* should be handled with particular caution). A total of 1 mL $HAuCl_4$ (1%) was added to 100 mL ultrapure water and heated to boiling with vigorous stirring. Then, 3 mL trisodium citrate (1%) was added with stirring and heated to boiling. The color of the solution changed from pale yellow to wine red in 1 min. The colloid was boiled for an additional 20 min. Finally, the heating source was removed and the system was allowed to cool to room temperature under stirring. The prepared AuNPs were stable for several months when stored in a clean container at room temperature.

Functionalization of the AuNPs with the thiol-modified cDNA was adapted from a previously reported protocol,[33,34] on the basis of the strong Au–S interaction between the gold lattice and the thiol group. All the glassware was allowed to soak in 12 M NaOH for 1 h, rinsed with ultrapure water, and oven-dried before use. A total of 1 μL TCEP (40 mM, pH 5.2) was added to 5 μL (20 μM) thiol-modified cDNA and incubated at 37 °C for 1 h to reduce disulfide bonds and activate the oligonucleotides. The TCEP-treated cDNA was added to 500 μL of the AuNPs with gentle shaking by hand and reacted in a darkroom under magnetic stirring at room temperature for at least 24 h. After that, 5 μL Tris acetate (500 mM, pH 8.2) buffer and 50 μL 1 M NaCl were added to the mixture with gentle hand shaking and stored in a darkroom at room temperature for at least 24 h. The resulting cDNA–AuNP nanoconjugates were centrifuged at 13 000 rpm at room temperature for 30 min, washed with 200 μL buffer (25 mM Tris acetate, pH 8.2, 100 mM NaCl) three times, and finally resuspended in 100 μL buffer (25 mM Tris acetate, pH 8.2, 300 mM NaCl) for subsequent experiments.

Cell lines and culture

CCRF-CEM cells (human acute lymphoblastic leukemia), HL-60 cells (human acute promyelocytic leukemia), and HeLa cells (human cervix adenocarcinoma) were obtained from Nanjing KeyGen Biotech Co. Ltd. CCRF-CEM and HL-60 cells were cultured in RPMI 1640 medium (Gibco, Grand Island, NY, USA) supplemented with 10% fetal calf serum (FCS; Sigma), penicillin (100 μg mL^{-1}), and streptomycin (100 μg mL^{-1}) at 37 °C in a humidified atmosphere containing 5% CO_2. At the logarithmic growth phase, the cells were collected and separated from the medium by centrifugation at 1000 rpm for 5 min, and washed twice with sterile PBS buffer (pH 7.4). The cells were suspended in sterile PBS buffer to obtain a homogeneous cell suspension with a concentration determined using a Petroff–Hausser cell counter (Hausser Scientific Partnership, Horsham, PA, USA). HeLa cells were cultured in DMEM (Gibco) supplemented with the same components as other cells.

Construction of the competitive hybridization-based sensing platform

The aptamer–Fe_3O_4 MNP/cDNA–AuNP nanoprobes were fabricated by base-pairing interactions. One hundred milliliters of aptamer–Fe_3O_4 MNP suspension was mixed with 100 mL cDNA–AuNP suspension for sufficient hybridization, which was carried out for 50 min at 37 °C in 100% humidity. The wine red cDNA–AuNP colloidal suspension turned pale red after cDNA–AuNPs were assembled on the surface of aptamer–Fe_3O_4 MNP nanoconjugates. After magnetic separation with an external magnet, the resulting nanoprobes were collected and washed three times with PBS buffer.

For the competition binding assay, 100 μL CCRF-CEM cell suspension was added to the aptamer–Fe_3O_4 MNP/cDNA–AuNP nanoprobes and incubated for 40 min at 37 °C in a humidified atmosphere containing 5% CO_2. The cells could be captured *via* the specific binding between aptamers and CCRF-CEM cells. The cell-captured nanoprobes were separated using an external magnet and washed three times with PBS buffer to remove the non-captured cells.

Silver-deposition enhancement was carried out on the cell-captured nanoprobes by reaction with a 50 μL 1 : 1 mixture of silver enhancer solution A and B for 5 min in a dark incubator. The system was washed thoroughly with deionized water to remove nonspecifically bound conjugates, fixed in 50 μL $Na_2S_2O_3$ (2.5%) solution for 4 min, separated using an external magnetic field, and rinsed thoroughly with deionized water again.

Electrochemical detection

The glassy carbon electrode (GCE) of 3 mm diameter was polished to a mirror using 0.3 and 0.05 μm alumina slurry (Buehler) followed by rinsing thoroughly with deionized water. The electrode was ultrasonicated in 1 : 1 nitric acid, acetone and deionized water, rinsed thoroughly with deionized water, and allowed to dry under nitrogen flow. After silver-deposition enhancement, the deposited silver remaining on the nanoprobes was dissolved by addition of 400 μL 1 M HNO_3. The resulting solution (400 μL) was transferred to 3 mL 0.2 M HAc–NaAc buffer (pH 5.2) to perform square wave anodic stripping voltammetric (SWASV) detection. The three-electrode system contained a GCE, a SCE and a platinum counter electrode. SWASV detection involved electrodeposition at −1.1 V for 120 s and stripping from −0.6 to +0.4 V under a N_2 atmosphere, using a square wave voltammetric waveform, with a 4 mV potential step, 25 Hz frequency, and an amplitude of 25 mV.

Calcein-AM staining procedure

For calcein-AM assay, 100 μL calcein-AM reagent was added to the CCRF-CEM cell-captured aptamer–Fe_3O_4 MNP/cDNA–AuNP nanoprobes, and incubated for 1 h at 37 °C in a humidified atmosphere containing 5% CO_2. The mixture was separated with an external magnet and washed three times with PBS buffer before detection.

Results and discussion

Characterization of the nanoprobe

The aptamer–Fe_3O_4 MNP/cDNA–AuNP nanoprobes were first characterized by SEM (Fig. 1A–C). The Fe_3O_4 MNPs were regular, spherical and well-dispersed with an average diameter of 320 nm (Fig. 1A). After the aptamer–Fe_3O_4 MNP/cDNA–AuNP nanoprobes were formed, a homogeneous distribution of plentiful, individual, and light AuNPs on the surface of the Fe_3O_4 MNPs was observed (Fig. 1B). After AuNP-catalyzed silver deposition, the nanoprobes were entirely covered by 3D coral-like silver aggregates (Fig. 1C). These changes demonstrate the effective fabrication of the nanoprobes.

Inverted fluorescence microscopy imaging and calcein-AM staining were used to observe the CCRF-CEM cells, which competed efficiently with AuNP-conjugated cDNA to bind specifically with the aptamers. In addition, calcein-AM changed to bright green fluorescent calcein when hydrolyzed by endocellular esterase in living cells, therefore, it was used for detecting cell viability.[35] As expected, the bright green fluorescence in Fig. 1D showed that the CCRF-CEM cells were successfully captured by the aptamer–Fe_3O_4 MNP/cDNA–AuNP nanoprobes, and an overwhelming majority of the captured cells were alive.

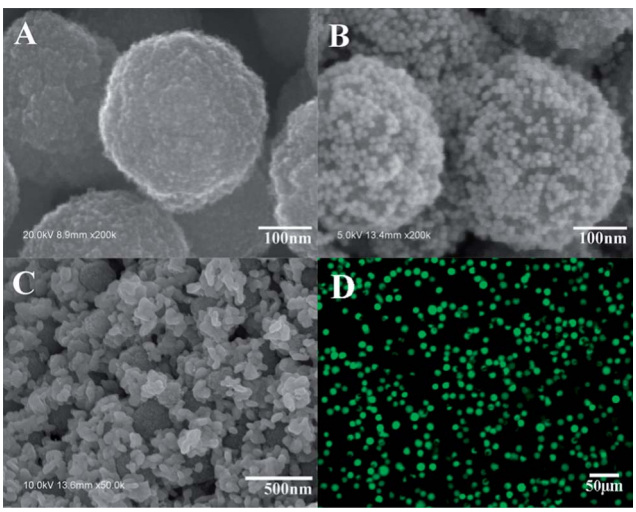

Fig. 1 SEM images of pure Fe_3O_4 MNPs (A), aptamer–Fe_3O_4 MNP/cDNA–AuNP nanoprobes (B), silver-deposition enhancement on the aptamer–Fe_3O_4 MNP/cDNA–AuNP nanoprobes (C), and the fluorescent image of the CCRF-CEM cells stained by calcein-AM after capture by the aptamer–Fe_3O_4 MNP/cDNA–AuNP nanoprobes (D). The living CCRF-CEM cells emitted bright green fluorescence.

Characterization of the aptamer–Fe_3O_4 MNP nanoconjugates

The aptamer–Fe_3O_4 MNP nanoconjugates were formed by a coupling reaction between the carboxyl group of Fe_3O_4 MNPs and the amino group of the aptamers. The FT-IR spectra were used to confirm the successful fabrication of the conjugates (Fig. 2). A strong transmission band around 583 cm^{-1} was attributed to Fe–O vibrations (curve B); the characteristic peak of the aptamer that appeared around 1061 cm^{-1} was due to C–N stretching vibrations (curve C); and both of the two characteristic peaks were retained in the aptamer–Fe_3O_4 MNP nanoconjugates (curve A). Two new vibration bands around 1644 and 1413 cm^{-1} clearly showed the formation of amido bonds after the coupling reaction (curve A). These results revealed that the amino-modified aptamers were successfully conjugated with the carboxyl-functionalized Fe_3O_4 MNPs.

Characterization of the cDNA–AuNP nanoconjugates

UV-vis absorption spectroscopy was used to monitor the functionalization of AuNPs with thiol-modified cDNA (Fig. 3). The pure AuNPs and cDNA showed a characteristic absorption peak at 520 nm (curve B) and 260 nm (curve C), respectively. After conjugation, two peaks were visible and the characteristic peak

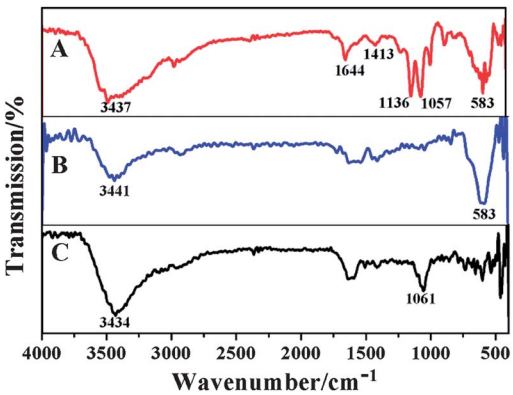

Fig. 2 FT-IR spectra of aptamer–Fe_3O_4 MNP nanoconjugates (A), pure Fe_3O_4 MNPs (B), and pure aptamers (C).

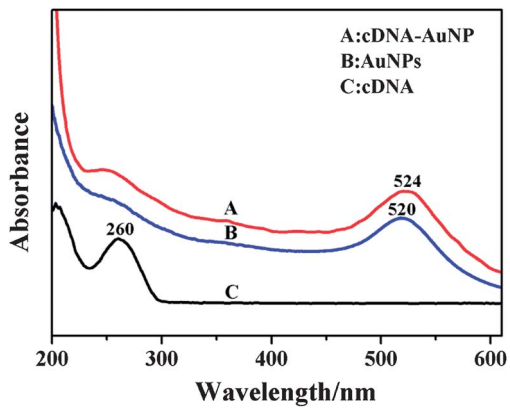

Fig. 3 UV-vis absorption spectra of cDNA–AuNP nanoconjugates (A), pure AuNPs (B), and pure cDNA (C).

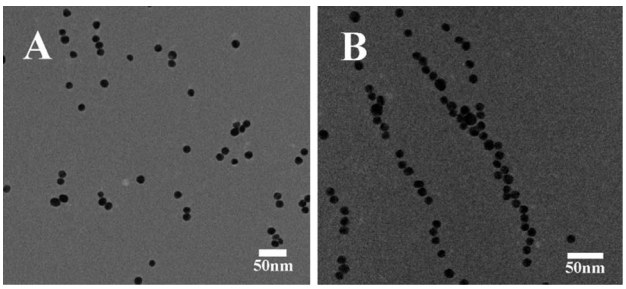

Fig. 4 TEM images of pure AuNPs (A) and cDNA–AuNP nanoconjugates (B).

of AuNPs underwent a 4 nm red shift to 524 nm (curve A), due to the interparticle plasmon coupling. The cDNA–AuNP nanoconjugates were also characterized by TEM images (Fig. 4). A pearl-necklace-like nanostructure was formed by the cDNA–AuNP nanoconjugates (Fig. 4B) by comparison with the pure well-dispersed AuNPs (Fig. 4A), indicating that cDNA acted as a bridge to connect AuNPs with each other. These results demonstrate the successful assembly of cDNA onto the AuNP surface.

Detection principle of the competitive hybridization-based sensing platform

The detection principle of the present competitive electrochemical sensing system is illustrated schematically in Scheme 1. An aptamer was designed to bind specifically to CCRF-CEM cells with high affinity, and an amino group was introduced to its 41-bp sequence from the 5′-terminal. A partial cDNA was designed to match the aptamer sequence and modified with a thiol group at its 5′-end. To fabricate the cytosensor, the amino-modified aptamers were first assembled on the surface of the carboxyl-functionalized Fe_3O_4 MNPs using EDC and NHS. The cDNA–AuNP nanoconjugates were prepared by the strong Au–S linkages between the gold lattices and the sulfur atoms of thiol-modified cDNA. After mixing the prepared AuNP-conjugated cDNA with the Fe_3O_4 MNP-bound aptamers for sufficient hybridization by base-pairing interactions, following magnetic separation, the aptamer–Fe_3O_4 MNP/cDNA–AuNP nanoprobes were successfully fabricated. In this way, the Fe_3O_4 MNPs acting as both the separation tool and the strong nanocarriers for loading AuNPs could amplify the detection signal.

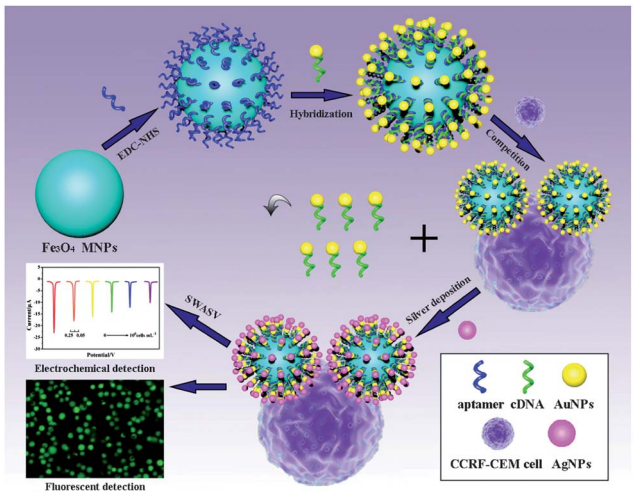

Scheme 1 Schematic illustration of the fabrication and measurement process of the competitive hybridization-based sensing platform.

For an aptamer, the consensus secondary structure motif upon a target molecule is a tertiary folding conformation, whereas, in the presence of a cDNA sequence, only a DNA duplex structure is formed. We assume that the aptamer is in a dynamic conformational equilibrium between the binding-competent tertiary folding conformer and the DNA duplex conformer. Furthermore, with a high-affinity aptamer (*e.g.*, CCRF-CEM-cell-specific aptamer), the strong binding interaction between the aptamer and the target molecule could compete favorably with the aptamer–cDNA binding interaction.[36,37] As a result, when target CCRF-CEM cells were introduced, the Fe_3O_4 MNP-bound aptamers preferred to form the aptamer–target complex rather than the aptamer–cDNA duplex, shifting the following equilibrium to the right, and some of the AuNP-conjugated cDNA was released from the nanoprobes:

$$\text{Fe}_3\text{O}_4\text{–aptamer}\cdot\text{cDNA–AuNP} + \text{target cell} \rightleftharpoons \text{Fe}_3\text{O}_4\text{–aptamer}\cdot\text{target cell} + \text{cDNA–AuNP} \quad (1)$$

After competitive binding, the dissociated cDNA–AuNP nanoconjugates as free, single-stranded elements were removed by magnetic separation. The residual AuNPs on the nanoprobes acted as catalysts for the reduction of silver ions as well as nuclei for the deposition of metallic silver.[29] The initial metallic silver nucleation on the AuNPs resulted in deposition of silver nanoparticles (AgNPs) on themselves, formation of large silver particles, and ultimately coverage of the entire nanoprobes. The silver amplification process further amplified the aptamer–target recognition event.

To transduce the target molecular recognition into a detectable electrochemical signal, the deposited AgNPs on the nanoprobes were dissolved in HNO_3 to produce a solution containing Ag ions for electrochemical detection using the SWASV method.

Optimization of the detection conditions

Aptamers form DNA duplex structures when binding to cDNA sequences, and adopt tertiary complex structures when binding to target molecules.[36,37] Incubation conditions, especially the time, have a significant impact on the dynamic conformational equilibrium of aptamers between the two distinct structures. Therefore, the incubation times for hybridization and competitive binding were investigated.

As shown in Fig. S1A,† the stripping peak current changed with the incubation time for Fe_3O_4 MNP-bound aptamers to hybridize with AuNP-conjugated cDNA. With increasing incubation time, the peak current increased and tended towards a stable value after 50 min, which indicated saturated hybridization between Fe_3O_4 MNP-bound aptamers and AuNP-conjugated cDNA. Thus, 50 min was chosen as the optimal hybridization time.

Fig. S1B† shows the effect of incubation time for CCRF-CEM cells (1.0×10^4 cells per mL) to compete with AuNP-conjugated cDNA to bind preferentially with Fe_3O_4 MNP-bound aptamers. The peak current decreased with increasing incubation time. This phenomenon can be explained in terms of the competitive nature of our detection principle. When the target cells were introduced, aptamers preferred to form aptamer–target complexes rather than aptamer–cDNA duplexes. The switch in the binding partners of the aptamers took place along with a significant decrease in the stripping peak current, owing to the release of the AuNP-conjugated cDNA. After 40 min, the current signal maintained an almost constant value, indicating an equilibrium state between the amount of free AuNP-conjugated cDNA and the amount of residual AuNP-conjugated cDNA on the nanoprobes. Therefore, 40 min was chosen as the favorable competitive binding time.

The silver deposition time is another key parameter that can affect the overall electrochemical signal, and it should also be optimized. Increasing the silver deposition time could enhance the stripping peak current. However, a longer deposition time could result in a higher background current.[38] Thus, the signal-to-noise ratio was used to optimize the deposition conditions so as to achieve a compromise between the background current and the target recognition-induced enhanced current. As shown in Fig. S1C,† the signal-to-noise ratio increased with deposition time until 5 min, and then it decreased quickly. Therefore, the optimal reaction time for silver-deposition enhancement was set at 5 min.

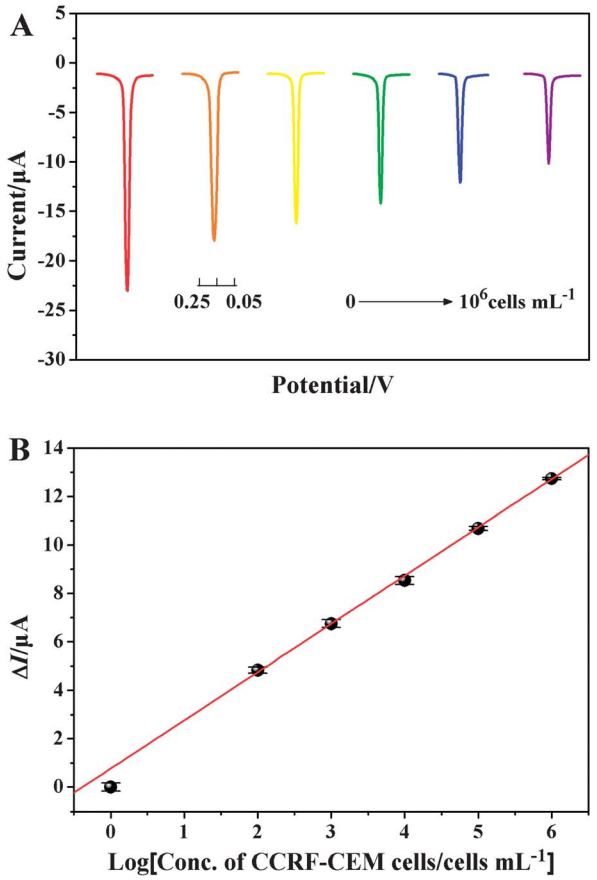

Fig. 5 Competition between CCRF-CEM cells and AuNP-conjugated cDNA for binding with Fe_3O_4 MNP-bound aptamers. (A) Square wave anodic stripping voltammograms for detecting CCRF-CEM cells at 0, 1.0×10^2, 1.0×10^3, 1.0×10^4, 1.0×10^5 and 1.0×10^6 cells per mL (left to right). (B) Corresponding linear calibration curve of the decreased current (ΔI) *versus* the logarithmic value of CCRF-CEM cell concentration. The error bars represent RSD from three independent experiments.

Analytical performance

To demonstrate that the developed competitive hybridization-based electrochemical cytosensor can be used for accurate quantification of target cells, the current responses to CCRF-CEM cells at various concentrations were evaluated by SWASV under the optimal experimental conditions. In this assay, target CCRF-CEM cells competed favorably with AuNP-conjugated cDNA to bind preferentially with high affinity to the Fe_3O_4 MNP-bound aptamers, releasing some of the AuNP-conjugated cDNA from the nanoprobes. As the target cell concentration increased, the amount of residual AuNPs on the nanoprobes gradually decreased, accompanied by a reduction in the deposited silver nanoparticles and stripping peak current. The difference in peak current (ΔI), was defined as $\Delta I = I_0 - I_{cell}$, where I_0 and I_{cell} represent the current measured in the absence and presence of the target cells at different concentrations, respectively. ΔI showed a decreasing trend with an increase in CCRF-CEM cell concentration (Fig. 5A). The corresponding calibration curve (Fig. 5B) showed a good linear relationship between ΔI and the logarithmic value of CCRF-CEM cell concentration in the range from 1.0×10^2 to 1.0×10^6 cells per mL, with a correlation coefficient of 0.9994.[39] The detection limit was 1.0×10^2 cells per mL, which was much lower than that of 1.0×10^4 mL^{-1} K562/ADM leukemia cells detected by electrochemical immunoassay using an AuNP–CS modified GCE,[40] and comparable to that of 2.5×10^2 mL^{-1} HeLa cells obtained from a peptide nanotube–folic acid-modified graphene electrochemical biosensor,[41] indicating relatively high sensitivity. One hundred microliters of CCRF-CEM cell suspension was required for the competition between target cells and cDNA, therefore, our detection method could detect as few as 10 cells. Such attractive high sensitivity was ascribed to the joint effects of the signal amplification strategy, by which the aptamer–target recognition event could be dramatically enhanced, and the necessary noise reduction measures that could assist to push down the detection limit.

Satisfactorily, our detection method also exhibited high reproducibility. At a CCRF-CEM cell concentration of 1.0×10^6 mL^{-1}, the electrochemical sensor yielded a reproducible signal with a relative standard deviation (RSD) of 3.8%. In addition, when the aptamer–Fe_3O_4 MNP/cDNA–AuNP nanoprobes were stored at 4 °C and detected intermittently every 3 days, the analytical performance did not show a significant difference after 30 days, demonstrating acceptable stability. The good stability might be attributed to the aptamers and Fe_3O_4 MNPs, which are both stable in an ambient environment. More importantly, owing to the magnetism of the Fe_3O_4 MNPs that allowed targets to be easily separated and enriched, the

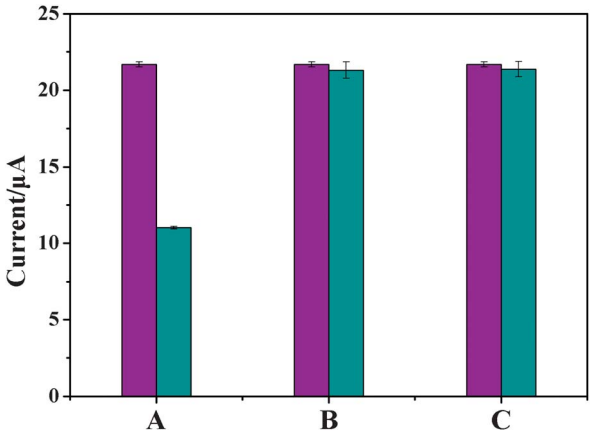

Fig. 6 Histograms of the specificity for detecting CCRF-CEM cells. The height of the columns represents the peak current of 0 cells per mL (A–C, purple), 1.0×10^5 mL^{-1} CCRF-CEM cells (A, blue), 1.0×10^5 mL^{-1} HL-60 cells (B, blue), and 1.0×10^5 mL^{-1} Hela cells (C, blue). The error bars represent RSD from three independent experiments.

proposed electrochemical cytosensor possessed a unique property of operational convenience.

Specificity of the electrochemical cytosensor

Specificity is one of the most important criteria for evaluating a detection method. To study the specificity of the proposed electrochemical detection system, the response of the assay to the non-target HL-60 and HeLa cells was investigated with the same experimental procedures as for the target CCRF-CEM cells. As shown in Fig. 6, the current response of the cytosensor corresponding to the addition of 1.0×10^5 mL^{-1} CCRF-CEM cells (A, blue) was much smaller than that of no cells (A, purple). When the cytosensor was incubated with 1.0×10^5 mL^{-1} HL-60 cells (B) or 1.0×10^5 mL^{-1} HeLa cells (C), no apparent current response decrease occurred. The excellent specificity should be ascribed to the intrinsic characteristics of the target-cell-specific aptamers, the competitive nature of the detection method, and the efficient magnetic separation by Fe_3O_4 MNPs to remove nonspecific cells, endowing the present electrochemical cytosensor with great potential to identify different cell types and reduce false-positive results.

Conclusions

In summary, we developed a novel aptamer-based competition strategy for highly selective and ultrasensitive electrochemical detection of leukemia cells with a detection limit down to 10 cells. On account of the intrinsic target-induced, structure-switching capability of each aptamer, the developed methodology could be easy to generalize and suitable for the development of aptamer-based sensing applications. This competitive, hybridization-based, electrochemical sensing platform integrated various functional elements into a collaborative detection method, achieving a synergistic effect of high sensitivity, good specificity, simple operability, rapid response, desirable reproducibility, and acceptable stability, showing great clinical value in the early diagnosis and prognosis of leukemia.

Acknowledgements

We are grateful for the support of the National Basic Research Program of China (Grant 2011CB933502) and the National Natural Science Foundation of China (Grants 21121091).

Notes and references

1 D. K. Graham, D. B. Salzberg, J. Kurtzberg, S. Sather, G. K. Matsushima, A. K. Keating, X. Liang, M. A. Lovell, S. A. Williams and T. L. Dawson, *Clin. Cancer Res.*, 2006, **12**, 2662–2669.
2 C. Brown, S. Larsen, H. Iland, D. Joshua and J. Gibson, *Int. Med. J.*, 2012, **42**, 1179–1186.
3 R. Paredes-Aguilera, L. Romero-Guzman, N. Lopez-Santiago, L. Burbano-Ceron, C. D. Monte and S. Nieto-Martinez, *Am. J. Hematol.*, 2001, **68**, 69–74.
4 S. K. Singh, C. Hawkins, I. D. Clarke, J. A. Squire, J. Bayani, T. Hide, R. M. Henkelman, M. D. Cusimano and P. B. Dirks, *Nature*, 2004, **432**, 396–401.
5 R. A. Ghossein and S. Bhattacharya, *Eur. J. Cancer*, 2000, **36**, 1681–1694.
6 L. Belov, O. de la Vega, C. G. dos Remedios, S. P. Mulligan and R. I. Christopherson, *Cancer Res.*, 2001, **61**, 4483–4489.
7 P. Paterlini-Brechot and N. L. Benali, *Cancer Lett.*, 2007, **253**, 180–204.
8 Z.-S. Wu, H. Zhou, S. Zhang, G. Shen and R. Yu, *Anal. Chem.*, 2010, **82**, 2282–2289.
9 X. Chen, K. Zhang, J. Zhou, J. Xuan, W. Yan, L.-P. Jiang and J.-J. Zhu, *Biosens. Bioelectron.*, 2010, **25**, 1130–1136.
10 D.-Q. Feng, G. Liu, W. Zheng, J. Liu, T. Chen and D. Li, *Chem. Commun.*, 2011, **47**, 8557–8559.
11 E. Largy, F. Hamon and M.-P. Teulade-Fichou, *Methods*, 2012, **57**, 129–137.
12 S. Choi and J. W. Kelly, *Bioorg. Med. Chem.*, 2011, **19**, 1505–1514.
13 A. Fallarero, K. Pohjanoksa, G. Wissel, U.-M. Parkkisenniemi-Kinnunen, H. Xhaard, M. Scheinin and P. Vuorela, *Eur. J. Pharm. Sci.*, 2012, **47**, 941–951.
14 K. Bernardeau, J. Kerzhero, A. Fortun, A. Moreau-Aubry, E. Favry, K. Echasserieau, E. Tartour, B. Maillère and F. Lang, *J. Immunol. Methods*, 2011, **371**, 97–105.
15 B. Srinivasan, Y. Li, Y. Jing, C. Xing, J. Slaton and J.-P. Wang, *Anal. Chem.*, 2011, **83**, 2996–3002.
16 N. Lu, C. Shao and Z. Deng, *Analyst*, 2009, **134**, 1822–1825.
17 Y. Jin, J. Bai and H. Li, *Analyst*, 2010, **135**, 1731–1735.
18 C. L. Hamula, H. Zhang, L. L. Guan, X.-F. Li and X. C. Le, *Anal. Chem.*, 2008, **80**, 7812–7819.
19 A. D. Ellington and J. W. Szostak, *Nature*, 1990, **346**, 818–822.
20 C. Tuerk and L. Gold, *Science*, 1990, **249**, 505–510.
21 Y. Xiao, B. D. Piorek, K. W. Plaxco and A. J. Heeger, *J. Am. Chem. Soc.*, 2005, **127**, 17990–17991.
22 H.-A. Ho and M. Leclerc, *J. Am. Chem. Soc.*, 2004, **126**, 1384–1387.
23 Y.-F. Huang, H.-T. Chang and W. Tan, *Anal. Chem.*, 2008, **80**, 567–572.
24 S. D. Jayasena, *Clin. Chem.*, 1999, **45**, 1628–1650.
25 S. Bi, Y. Yan, X. Yang and S. Zhang, *Chem.–Eur. J.*, 2009, **15**, 4704–4709.

26 S. Gupta, S. Huda, P. K. Kilpatrick and O. D. Velev, *Anal. Chem.*, 2007, **79**, 3810–3820.
27 M. R. Akanda, M. A. Aziz, K. Jo, V. Tamilavan, M. H. Hyun, S. Kim and H. Yang, *Anal. Chem.*, 2011, **83**, 3926–3933.
28 J.-J. Zhang, T.-T. Zheng, F.-F. Cheng, J.-R. Zhang and J.-J. Zhu, *Anal. Chem.*, 2011, **83**, 7902–7909.
29 P. M. Lackie, *Histochem. Cell Biol.*, 1996, **106**, 9–17.
30 X. Chu, X. Fu, K. Chen, G.-L. Shen and R.-Q. Yu, *Biosens. Bioelectron.*, 2005, **20**, 1805–1812.
31 W. Sheng, T. Chen, R. Kamath, X. Xiong, W. Tan and Z. H. Fan, *Anal. Chem.*, 2012, **84**, 4199–4206.
32 S. Liu, F. Lu, R. Xing and J. J. Zhu, *Chem.–Eur. J.*, 2011, **17**, 620–625.
33 G. Qiao, Y. Gao, N. Li, Z. Yu, L. Zhuo and B. Tang, *Chem.–Eur. J.*, 2011, **17**, 11210–11215.
34 J. Liu and Y. Lu, *Nat. Protocols*, 2006, **1**, 246–252.
35 T.-T. Zheng, R. Zhang, L. Zou and J.-J. Zhu, *Analyst*, 2012, **137**, 1316–1318.
36 R. Nutiu and Y. Li, *J. Am. Chem. Soc.*, 2003, **125**, 4771–4778.
37 N. Hamaguchi, A. Ellington and M. Stanton, *Anal. Biochem.*, 2001, **294**, 126–131.
38 D. Lin, J. Wu, M. Wang, F. Yan and H. Ju, *Anal. Chem.*, 2012, **84**, 3662–3668.
39 J.-Y. Park, Y.-S. Lee, B. H. Kim and S.-M. Park, *Anal. Chem.*, 2008, **80**, 4986–4993.
40 D. Du, H. Ju, X. Zhang, J. Chen, J. Cai and H. Chen, *Biochemistry*, 2005, **44**, 11539–11545.
41 J. J. Castillo, W. E. Svendsen, N. Rozlosnik, P. Escobar, F. Martínez and J. Castillo-León, *Analyst*, 2013, **138**, 1026–1031.